ADER-DG with a-posteriori finite-volume limiting to simulate tsunamis in a parallel adaptive mesh refinement framework

Leonhard Rannabauer [a],*, Michael Dumbser [b], Michael Bader [a]

[a] *Department of Informatics, Technical University of Munich, Bolzmannstr. 3, Garching 85748, Germany*
[b] *Department of Civil, Environmental and Mechanical Engineering, University of Trento, Via Mesiano, 77, Trento 38123, Italy*

ARTICLE INFO

ABSTRACT

In this paper we present the application of the ADER Discontinuous Galerkin method with an *a-posteriori* Finite-Volume limiter on the simulation of tsunamis. Goal is to obtain a method of high-order convergence in deep water areas while being able to handle wetting & drying at coast lines. Several adjustments of the original ADER-DG method are presented to preserve characteristics like the well-balanced property. We evaluate and confirm developed concepts by a series of numerical tests and present them in the context of reconstructed tsunamis.

1. Introduction

High-order discretization methods are a highly valuable counterpart to current high performance computing (HPC) architectures. They increase the achieved accuracy per invested degree of freedom, while also rising arithmetic intensity. Especially the latter makes high-order methods more convenient for modern HPC architectures, as bandwidth and latency of main memory is falling behind the peak performance of multiple compute cores. In this paper, we adapt a high-order discontinuous Galerkin discretization for the Shallow Water equations (SWE) to make it suitable for the simulation of tsunamis.

There are several criteria posed for a proper numerical scheme to model tsunamis. For example the well-balanced property demands that resting lake scenarios need to be kept exactly constant as tsunamis in a wide domain are only small perturbations of such solutions. The most crucial and on the other hand problematic aspect is modeling inundation in coastal areas. For Finite-Volume methods (FV) this problem is well explored and sufficiently solved by elaborate and effective limiting schemes like the set of augmented Riemann solvers by D. George [1] or HLLE approximate Riemann Solvers as [2] by Delis, which are well-balanced and hold desirable properties like positivity preservation. For Discontinuous Galerkin (DG) methods however there only exists a sparse number

of methods, for example the second order Runge Kutta DG (RK-DG) method by Vater et al. [3] based on a Barth Jespersen type limiter, or the RK-DG approach of high-order, by Bunya [4].

A different approach is the Arbitrary High-Order Discontinuous Galerkin (ADER-DG) method proposed by Dumbser et al. in [5]. It follows the main paradigm of reaching high-order convergence *element-locally*. The scheme solves integration in time without considering influences along element interfaces and then reverts that abstraction by preforming a single correction step. To solve known high-order issues as Gibbs phenomenon a corresponding *a-posteriori* sub-cell limiter was present by Dumbser et al. in [6]. This limiter differs from known methods in an important aspect. Limiting is not performed by manipulating the computed solution but by detecting and revoking problematic DG solution candidates and recomputing them with a Finite-Volume scheme.

Our paper can be seen as the description of a distinct and adjusted application of the ADER-DG method with its novel limiter on the SWE. Different from already performed applications of the method on SWE as in [7] by Dumbser et al., we tailor the specification of ADER-DG and the limiting scheme to fulfill constraints given by tsunami simulation. Wetting & drying, which only few high-order methods are able to resolve, is performed by the corresponding limiter. This allows us to solve demanding problems and real applications as the reconstruction of tsunamis, which we will present in the last chapter.

The use of high-order ADER-DG is also motivated by the already mentioned trend of recent HPC architectures towards relatively higher computational power compared to memory speed. By

* Corresponding author.
  E-mail addresses: rannabau@in.tum.de (L. Rannabauer), michael.dumbser@unitn.it (M. Dumbser), bader@in.tum.de (M. Bader).
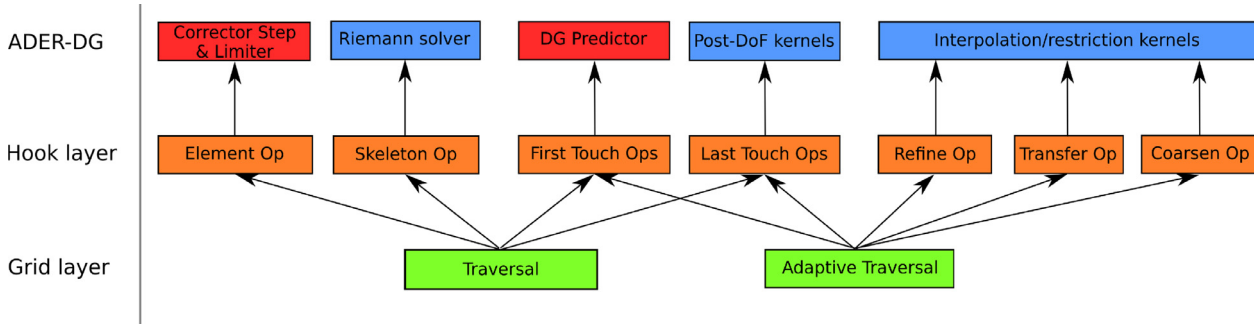
Fig. 1. Layer concept in sam(oa)^2 : Single traversals (in green) are hidden behind a hook concept (in orange), providing interfaces for operations on elements, boundaries, faces and more. The concrete implementation of ADER-DG (in red & blue) allows a numerical scheme of high-order, only needing two traversals of the grid. (For interpretation of the references to colour in this figure legend, the reader is referred to the web version of this article.)

being element local ADER-DG and its limiter allows to keep arithmetic intensity high. Together with using memory efficient grid traversal schemes that exploit space-filling curves, which we use in the encapsulating framework sam(oa)^2 [8], ADER-DG holds one big advantage compared to RK-DG: The time integrator of ADER-DG can be computed in a single traversal. In contrast RK-DG methods have to evaluate every intermediate k-stage of the semi-discrete scheme. As every stage depends on the previous, the whole grid has to be traversed again, for a RK method of order *N* we require at least *N* traversals.

In Section 2 we will summarize the sam(oa)^2 framework with its layer concept. The high-order ADER-DG scheme with its DG-Predictor and Corrector step will be presented in Section 3. Here we will also show how we achieve a well-balanced numerical scheme by evolving the source term. Section 4 will present our usage and customization of the *a-posteriori* FV limiter to resolve wetting & drying shorelines. The last two Sections 5 and 6 verify our concepts by a series of numerical tests and show application examples on reconstructed tsunamis.

2. The sam(oa)^2 framework

Code base for the implementation of our numerical scheme is the sam(oa)^2 framework developed by Meister et al. [9]. The framework is capable of shared and distributed memory parallelisation and adaptive mesh refinement (AMR) along wave fronts. Spatial discretization is strictly done by triangular meshes, where refinement and coarsening are achieved by newest vertex bisection [10]. The resulting mesh is always equivalent to a binary refinement tree and can be traversed by Sierpinski space filling curves (SSFC). To support the iterative formulation of FV and DG methods sam(oa)^2 manages persistent and temporary data and shares data between single elements over edges and nodes, where numerical fluxes or information for limiting schemes are computed and exchanged. SSFCs produce the key property that edges and nodes in the whole domain are accessed the last time in reverse order as they were accessed the first time. By this stack like behaviour redundant data accesses can easily be avoided. The iteration can be implemented in a cache-efficient way. For more information on SSFCs we refer to [11].

The interface of sam(oa)^2 for element-oriented discretization schemes, such as FV or DG methods, is built on a set of function hooks which hide the details of mesh traversals and provide the model developer with an element oriented interface to realize simulations of two dimensional systems of hyperbolic PDEs. The concept and our utilization is displayed in Fig. 1. The *element-local* nature of ADER-DG and its limiter allows us to implement a single time step by traversing the whole grid only two times. Elementary steps that will be described in Section 3 are the *Corrector and Lim-*

iting step, and the *DG-Predictor*, both marked by red boxes. As both of these steps require information from neighbouring elements of the respective other, we need to calculate them in two separate traversals. For AMR we are able to hide the calculation of the *DG-Predictor* step behind the mesh refining traversal.

3. Well-balanced numerical scheme

Our numerical scheme relies on the ADER-DG method proposed in [5] by Dumbser et al. Compared to DG approaches, as in [12] by Giraldo et al. or [13] by Xing et al., where the semi-discrete scheme is integrated in time by the Runge–Kutta (RK) method, ADER-DG uses a unique element-local predictor-corrector pattern.

3.1. Shallow water equations

The system of Partial Differential Equations (PDEs) we use to model oceanic waves are the well known two-dimensional Shallow Water Equations (SWE) in conservative formulation,

$$\mathbf{Q}_t + \nabla \cdot \mathbf{F}(\mathbf{Q}) - \mathbf{S}(\mathbf{Q}) = 0. \tag{1}$$

Here $(\nabla \cdot \mathbf{F}(\mathbf{Q}))_i = \sum_j \frac{\delta F_{ij}}{\delta x_j}$ denotes the divergence operator. Regarded physical quantities **Q** are water depth *h* as vertical distance between water level and bottom, and discharges in *x* and *y* direction, *hu* and *hv* as product of water depth and velocity. Flux **F**(**Q**) and source **S**(**Q**) terms are defined as:

$$\mathbf{Q} = \begin{pmatrix} h \\ hu \\ hv \end{pmatrix}, \quad \mathbf{S}(\mathbf{Q}) = \begin{pmatrix} 0 \\ ghb_x \\ ghb_y \end{pmatrix},$$

$$\mathbf{F}(\mathbf{Q}) = \begin{pmatrix} hu & hv \\ \frac{1}{2}gh + hu^2 & huv \\ huv & \frac{1}{2}gh + hv^2 \end{pmatrix}. \tag{2}$$

While the flux term considers conservation of mass and momentum, and hydrostatic pressure with gravitational acceleration *g*, the source term models the bottom topography or bathymetry *b*. Other influences like bottom friction or Coriolis force are omitted.

3.2. The ADER-DG method

In this section we summarize the mathematical theory behind the ADER-DG method and show what choices we made for its concrete implementation. For a detailed introduction we refer to the original paper by Dumbser et al. [5].

3.2.1. DG-predictor step

Integration in time is solved by a special weak form of the PDE.

$$\int_{t_n}^{t_{n+1}} \int_T \boldsymbol{\phi}^T \left(p_t + \nabla \cdot \mathbf{F}(p) - \mathbf{S}(p) \right) dxy \, dt = 0 \tag{3}$$

Compared to other DG approaches, the weak from is built on a set of test functions $\boldsymbol{\phi} = (\phi_i)_{i \in \mathbf{N}}$ defined on prisms in space and time, $T \times [t_n, t_{n+1}]$. As the convergence rate is determined only by the polynomial degree of the spatial and temporal approximation, the method's order is called as "arbitrary high".

Eq. (3) results in a non-linear equation system that can be evolved into an element-local fix-point iteration, which is proven to converge for a suitable CFL condition. The initial condition of the iteration only depends on the numerical solution at the current time step t_n. Result is the so-called DG-Predictor p which represents the element-local evolution of the PDE without considering effects of fluxes over the element boundaries.

In our method we implemented this iteration according to the following specification:

- As basis functions we choose the alpha optimized nodal Lagrange polynomials on triangles $\phi = (\phi_i)_{i \in N}$, described by Hestaven et al. in [14]. To obtain a basis on space-time prisms we build the tensor with the one dimensional Legendre Gauss Lobatto polynomials.
- By using the interpolation rule given by the set of Lagrange polynomials, occurring flux and source integrals can be transformed into matrix–matrix multiplications. The whole iterative method is developed into a quadrature free formulation. These matrices are similar to known mass and stiffness matrices, now defined in space-time.
- We repeat the iterative scheme until the relative change is lower than 10^{-14}.

3.2.2. The corrector step

As the DG-Predictor only represents an element-local evolution of the PDE, fluxes over boundaries need to be taken into account to get a valid time stepping scheme. This *Corrector step* is derived from a weak form on spatial test functions, considering the previously calculated predictor step. After integration by parts of the approximation in time and the flux term in space its formulation results in

$$\int_T \phi^T \phi \, dxy \, (\vec{q}_{n+1} - \vec{q}_n) + \sum_{i=1}^3 \int_{t_n}^{t_{n+1}} \int_{\delta T_i} \boldsymbol{\phi}^T D^-(p, p_i) \, \mathbf{n}_i \, dxy dt$$

$$- \int_{t_n}^{t_{n+1}} \int_T \nabla \cdot \boldsymbol{\phi}^T \mathbf{F}(p) - \boldsymbol{\phi}^T \mathbf{S}(p) \, dxy dt = 0 \tag{4}$$

and gives us a full time marching scheme for the degrees of freedom $\vec{q}_n$.

Fluxes between neighbouring elements are now considered, as the numerical solution to the Riemann problem on the space-time face, denoted by $D^-(p, p_i) \, \mathbf{n}_i$, is approximated. The solution depends on both neighbouring predictors p.

In our implementation we followed the same concepts of interpolation and quadrature as described in the previous chapter. As we assume that discontinuities are limited and the ADER-DG method will only be applied in smooth cases we chose a simple Rusanov Flux to solve the Riemann problem. We point to possibly more efficient solvers like newly developed HLLE solvers, e.g. in [15] by Leveque et al.

3.2.3. Well-balanced property through source decomposition

One of the main requirements on our numerical scheme is the preservation of equilibrial states. For tsunami simulation, the lake at rest scenario, which models an initial constant water level $H =$ $h + b = $ const. and zero velocities $u = v = 0$ should stay constant in time, independent of the bottom topography. This well-balanced property is in fact where the analytic source term of Eq. (2) originates from. In their original form the quadrature free formulation of (3) and (4) both violate this constraint and artificial waves arise that might obscure the observed tsunami.

$$\int_{t_n}^{t_{n+1}} \int_T \nabla \cdot \phi^T \phi \, \mathbf{F}(\vec{p}) - \phi^T \phi \, \mathbf{S}(\vec{p}) \, dxy \, dt \neq 0 \tag{5}$$

To keep the scheme well-balanced, we evolve the source integral into a representation similar to the flux integral. By using integration by parts,

$$\int_{t_n}^{t_{n+1}} \int_T \phi^T \mathbf{S}(p) \, dxy \, dt \approx \int_{t_n}^{t_{n+1}} \int_T \phi^T \phi \left(0, -gh\bar{H}_x, -gh\bar{H}_y \right) dxy \, dt$$

$$+ \int_{t_n}^{t_{n+1}} \int_{\delta T} \phi^T \phi \left(0, \frac{1}{2}g\vec{h^2} \cdot n_2, \frac{1}{2}g\vec{h^2} \cdot n_3 \right) dxy \, dt$$

$$+ \int_{t_n}^{t_{n+1}} \int_{T/\delta T} \phi_x^T \phi \left(0, \frac{1}{2}g\vec{h^2}, 0 \right) dxy \, dt$$

$$+ \int_{t_n}^{t_{n+1}} \int_{T/\delta T} \phi_y^T \phi \left(0, 0, \frac{1}{2}g\vec{h^2} \right) dxy \, dt. \tag{6}$$

The second, third and fourth term are always equivalent to hydrostatic pressure in the discrete formulation of the flux term. In the implementation we can thus omit them. Remaining terms vanish for resting domains, the numerical solution stays constant.

4. Wetting & Drying by an *a-posteriori* Finite-Volume limiter

The recently developed *a-posteriori* Finite-Volume limiter by Dumbser et al., presented in [6], extensively differs from known limiting schemes as slope limiters, presented in [14]. Problematic solutions are not manipulated but discarded and replaced by a newly computed FV solution.

We utilize this limiter to solve the two main issues of tsunami simulation with high-order schemes: Oscillations and wetting & drying.

4.1. The a-posteriori *Finite-Volume limiter scheme*

The original description of the limiter, from [6] can be summarized by the following work flow:

1. **Computation of a Candidate Solution.** Using the ADER-DG method compute for each cell a candidate solution $^*q^{n+1}$ at time t_{n+1}.
2. **Detecting troubled Cells.** The candidate solution gets tested by two conditions: Whether the cell fulfills physical constraints and the so called *discrete maximum principle*. If this is not the case the DG solution is considered as failed.
3. **Correcting troubled cells.** When a cell is problematic, the candidate solution is discarded. Solutions at time t_n for triangle T and all its adjacent neighbors T_i are converted to FV patch representations v^n and $v^{(n,i)}$. The Finite-Volume solution at the next time step v^{n+1} is computed using a robust scheme.
4. **Reconstructing the DG-Solution.** The final approximation q^{n+1} at time t_{n+1} is reconstructed from the new computed FV solution v^{n+1}. For untroubled cells the candidate solution is taken.

Finite-Volume patches are chosen to have an order of $2N+1$, where N is the polynomial degree of the DG approximation. This is the smallest possible cell size that does not violate the *CFL-Condition* for the prescribed DG time step size. Patches for ADER-DG methods of polynomial degree one, two and four can be seen in Fig. 2

The *discrete maximum principle* is described in detail in [6]. It detects oscillations by assuming that the solution in a cell must
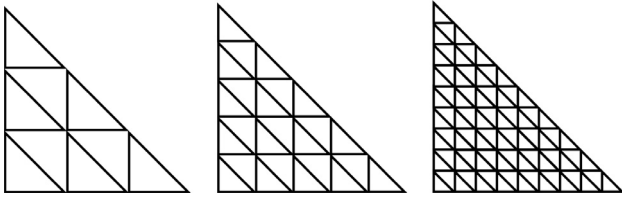
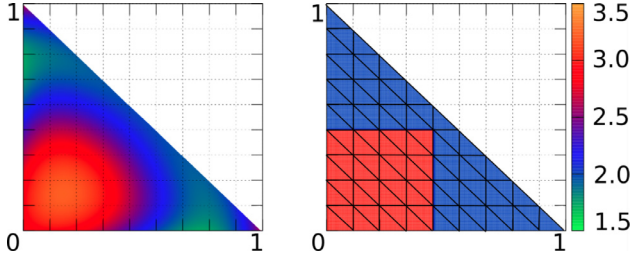**Fig. 2.** Finite-Volume patches for ADER-DG-1, ADER-DG-2 and ADER-DG-4.

Fig. 3. Reconstructed DG solution on the left from a Finite-Volume patch holding a discontinuity on the right.

Fig. 4. L1-Errors for the convergence scenario. All methods show high-order convergence of $\mathcal{O}(h^{n+0.5})$.

lie between the maxima and minima of itself and all its neighbours at the previous time step. This algorithm provides a simplified method which again follows element-locality as it only requires values of the previous time step that can be exchanged during the solution of the Riemann problem. Price for the simplicity is the risk of false detection, as accelerations through source terms violate the principle.

Projection from DG approximation to FV patch is done by averaging the polynomial over all sub-cells s_i,

$$v^n = \left(\frac{1}{|s_i|} \int_{s_i} q^n \, dxy \right)_{i=1..(2N+1)}. \tag{7}$$

By precomputing averages of all basis polynomials, projection can be reduced to a simple matrix–matrix multiplication.

Reconstruction of the DG polynomial at the next time step q^{n+1} from values of a FV patch v^{n+1} is performed by solving a constrained optimization problem. The reconstructed polynomial q^{n+1} is supposed to hold the average value for each sub-cell s_i,

$$\left\| \left(\frac{1}{|s_i|} \int_{s_i} q^{n+1} \, dxy - v_i^{n+1} \right)_i \right\|_2 = \min. \tag{8}$$

To keep conservation laws on single elements it is compulsory that the approximation keeps the volume on the whole triangle,

$$\int_T q^{n+1} \, dxy \overset{!}{=} \sum_{i=1}^{(2N+1)^2} |s_i| \cdot v_i^{n+1}. \tag{9}$$

By finding the derivative of the constrained least squares problem and solving for its unique root the DG polynomial is reconstructed. Precomputing the inverse of the resulting equation system reduces the process to a matrix–matrix multiplication. Fig. 3 shows the reconstruction of a polynomial of degree 4, the FV patch on the right models a discontinuity, the reconstructed polynomial can't represent that state exactly.

4.2. Application of the limiter on wetting & drying cells

While it is a key part of tsunami simulations, wetting & drying (in general also known as *positivity preservation*) in high-order DG methods is still an unresolved task. The limiting scheme allows us to use solutions to this problem which are only defined for FV methods: By using the augmented Riemann solver, by George
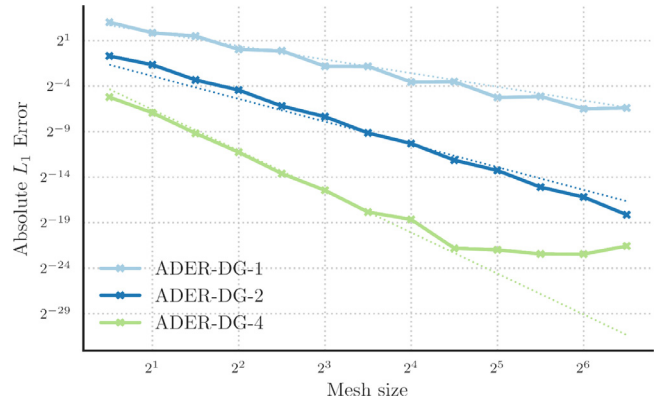
[1] within the FV limiter, we are able to model wetting and drying coasts and keep the high-order scheme in open-ocean areas.

Our implemented version of the limiter varies from the original formulation [6] in a few aspects:

- As physical constraint we set a constant water height threshold below which we consider cells as dry or becoming dry.
- Cells that are dried after correction by the FV method are not reconstructed as we assume only a small fraction of cells would be flooded in the next time step. We therefore don't compute candidate solutions for these cells.
- As reconstruction is a non-linear process, artificial waves might occur in the case of a constant water level with non-constant bathymetry. To keep constant water levels we always reconstruct water level first and then obtain water height by subtracting the bathymetry. A detailed discussion on this topic can be found in [16]

When simulating tsunamis we expect the majority of modeled land to remain dry. Preselecting dry cells saves the calculation of the ADER-DG scheme for those and directly applies the FV method.

5. Numerical tests

In this chapter we will present a series of numerical tests to validate our method.

5.1. Basic convergence order test

Due to the lack of two dimensional smooth analytic solutions we prove high-order convergence of our scheme by taking the one dimensional solution from [17] and transforming it on all lines $x - y = const.$ for arbitrary constants.

$$h(x,t) = \left(x^{-1} + e^{-t} \right) \cdot g$$
$$u(x,t) = x \tag{10}$$
$$b(x,t) = \left(\frac{-0.5 \cdot x^2}{g} + \frac{-g}{x} \right)$$

To avoid effects from boundary conditions only cells within a sufficiently small inner area of the domain are considered. Fig. 4 shows the absolute L_1-Error approximated by a suitable quadrature rule for mesh sizes from 2^0 to 2^7. ADER-DG-n denotes the ADER-DG method using degree n polynomials for spatial and temporal approximations. *Ideal* error graphs are hinted by a dotted plot in the respective color. Results show that our scheme reaches the expected numerical high-order convergence of $\mathcal{O}(h^{n+0.5})$ down to machine precision for ADER-DG-4.
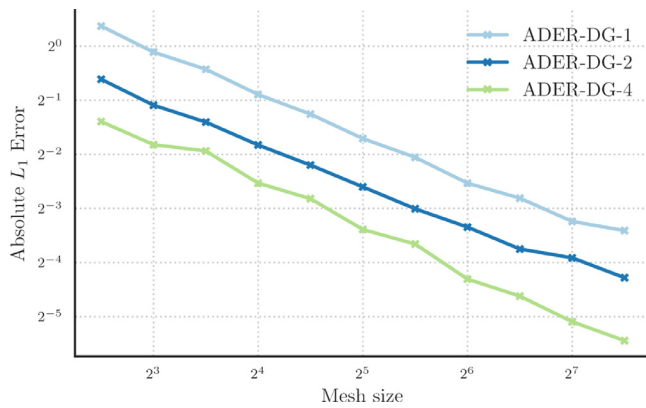
Fig. 5. L1-Errors for the limited all rarefaction solution.

Table 1
Fraction of limited cells for ADER-DG-1,ADER-DG-2 and ADER-DG-4 in the all rarefaction scenario.

Mesh Size	ADER-DG-1	ADER-DG-2	ADER-DG-4
2^3	0.35	0.42	0.35
2^5	0.16	0.23	0.14
2^7	0.05	0.07	0.04
2^8	0.04	0.03	0.02

5.2. Well-balanced property

To prove the well-balanced property of our numerical scheme we follow the lake at rest scenario from [18]. Bathymetry is modelled by an exponential function b.

$$-\log(b(x,y)) = x^2 + 2 \cdot xy + y^2 \qquad (11)$$

Water height is set to $h(x,y) = 5 - b(x,y)$, initial velocities are zero. Domain is the unit square around $(0,0)$. Meshed by a grid size of 2^6 we thus have around 7.5×10^5 elements. We choose a simulation time of 25 s which is around 1000 time steps for ADER-DG-4. L_1-errors of ADER-DG-1,ADER-DG-2 and ADER-DG-4 show that the methods keeps the resting lake solution sufficiently accurate:

ADER-DG-1	ADER-DG-2	ADER-DG-4
4.25−15	6.28e−15	3.60e−13

5.3. Discontinuous test

To show how effective our limiter is in the case of a traveling discontinuity, we tested our method for several mesh sizes against the *all rarefaction* benchmark from [15], with initial conditions

$$h_0(x) = 1$$

$$u_0(x) = \begin{cases} -0.5, & \text{for } x < 0 \\ 0.5, & \text{for } x > 0. \end{cases} \qquad (12)$$

We again rotate the one dimensional analytic solution into the two dimensional space by projecting it on lines $x - y = const$. The L_1-error is computed at $t = 0.1$. In the unlimited case our methods ADER-DG-1 to ADER-DG-4 diverge as expected due to Gibbs phenomenon. For the limited case, errors are shown in Fig. 5. All three methods converge linearly. The average fraction of limited cells in a single time step for several mesh sizes are shown in Table 1, and lead to the conclusion that the number approximately depends linearly on the mesh size.

This test shows one of the strengths of this limiter. While the detection algorithm for oscillations is very basic compared to other established limiters, it still only limits a small fraction of elements to hold convergence of the method.

5.4. Oscillating lake

The oscillating lake scenario, as proposed in [19], states a demanding benchmark for wetting & drying algorithms. The analytic solution to this problem is known, and given by the periodic formulation:

$$h(x,y,t) = \max(0, 0.05 \cdot (2 \cdot x \cos(\omega t) + 2 \cdot y \sin(\omega t))$$
$$+ 0.075 - b(x,y))$$
$$u(x,y,t) = 0.5 \cdot \omega \sin(\omega t)$$
$$v(x,y,t) = 0.5 \cdot \omega \cos(\omega t)$$
$$b(x,y) = 0.1 \cdot (x^2 + y^2), \qquad (13)$$

where $\omega = \sqrt{0.2 \cdot g}$. By periodicity of the trigonometric terms the solution is equivalent for all $t \equiv \hat{t} \mod 2\pi/\omega, \hat{t} \in [0, 2\pi/\omega)$. For our method this states a highly critical benchmark as the wet-drying front continuously moves through the domain. Our method has to adapt this moving front accurately to avoid drying cells in the DG case. The numerical solution by an ADER-DG-4 method is shown in Fig. 6, where the critical water height below which we switch to the Finite-Volume method is set to 0.001. The upper row shows the movement of the water height for 4 distinct time steps in one period. First and last picture show the solution at simulation time 0 and $2\pi\omega$ and are equivalent as in the analytic solution. The lower row shows whether the simulation is done by ADER-DG or on a Finite-Volume patch. We see that the area simulated by ADER-DG method moves with the water droplet through the domain. Both methods are in step and work harmonic as the solution remains equivalent after one period. To validate convergence, a series of tests was run. Snapshots of the simulation after five periods of the analytic solution were taken. The L_1 error norm by used degree of freedom for ADER-DG 1 to 4 can be seen in Fig. 7 and prove numerical convergence. To compare results the native FV method, used in the limiting scheme, with Euler time stepping and augmented Riemann solver is displayed. The comparison confirms our assumption: ADER-DG with FV limiter results in higher accuracy than a plain FV method.

6. Simulation of tsunami events

Main application area of our method is the simulation of tsunamis. In this chapter we present the reconstruction of two recent events, the Tohoku tsunami originating in the Japan trench of 2011 and the Sumatra tsunami in the Indian Ocean of 2004. Waves are generated by tracking the vertical displacement of bathymetry over time and translating the change directly to water height. This method neglects horizontal accelerations due to movement of the topography. While the initial ocean-floor displacement of the Tohoku tsunami is modelled by Okada's method [20] and provided by Galvez et al. [21], input for the Sumatra tsunami is the result of a dynamic rupture Earthquake simulation as described in [22] by Uphoff et al. Bottom topography in both cases is given by the GEPCO data set (http://www.gebco.net), which provides data with a detail of 30′ (roughly 900 m).

Along coasts we choose a threshold of 1km below which we switch to FV patches. This relatively high threshold has one main reason: Numerical results will only be compared to observations on the open ocean. Test showed that the threshold can be set down to the width of the largest element along the shoreline. After that point the iterative DG-Predictor scheme might diverge due to an unbound flux function.

An exemplary plot can be seen in Fig. 11, where the bathymetry is diffusely hinted in the background. Gray areas indicate that FV patches are used to simulate land and coast regions, while the blue area indicates the ADER-DG method in the wide ocean. The ADER-DG-4 solution of the Tohoku tsunami itself can be seen
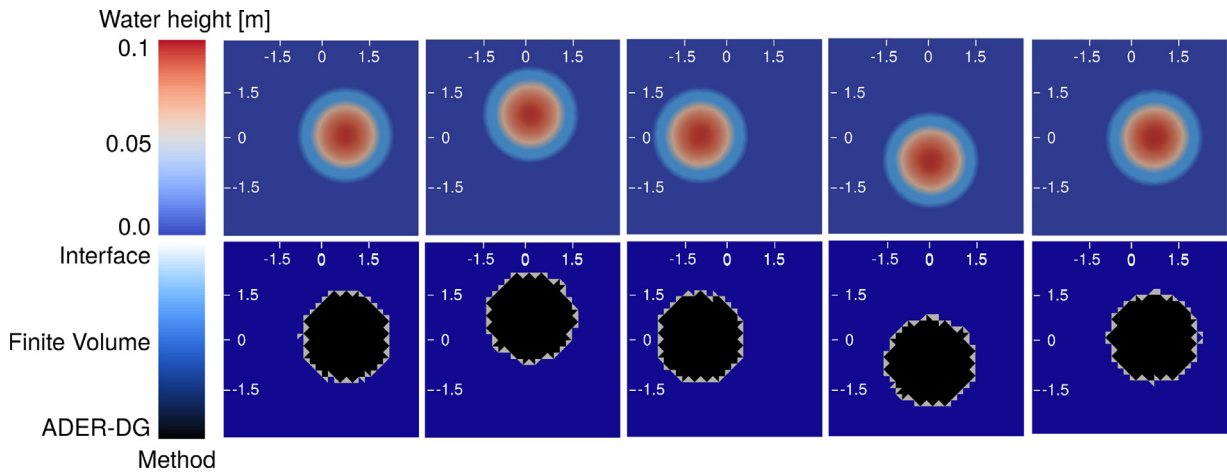
Fig. 6. Oscillating Lake simulated with ADER-DG-4. Top row of pictures shows the water height for time steps $0, \frac{1}{2}\pi\omega, \pi\omega, \frac{3}{2}\pi\omega, 2\pi\omega$. Lower row shows if the ADER-DG or FV method is used in the respective area.
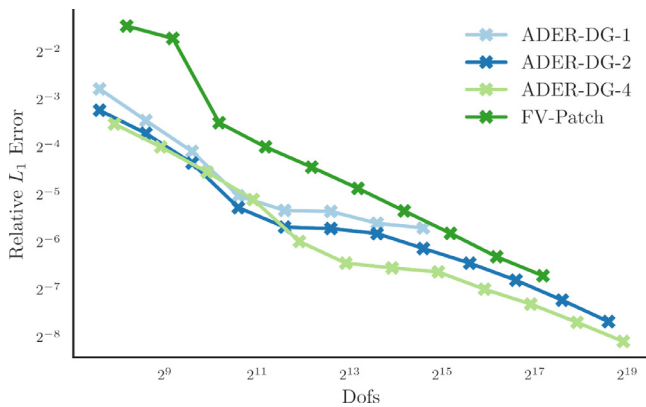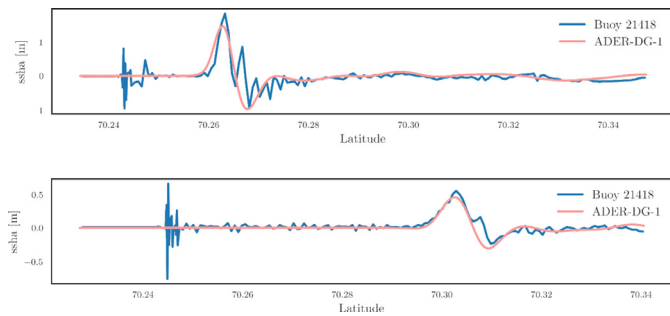

Fig. 7. L1-Error for the oscillating lake scenario.

Fig. 8. Comparison of real buoy data to numerical results for the Tohoku tsunami.

Fig. 9. Comparison between recorded satellite and numerical data for the Sumatra tsunami after 120 min.

Fig. 10. Tohoku tsunami after 60 min.

after 60 min in Fig. 10. To verify the accuracy of our numerical method, results are compared to measurements of sea surface height anomalies (ssha) by two buoys in front of the Japan coast of the day of the event. Both comparisons can be seen in Fig. 8 and show that the amplitude of the wave is reconstructed accurately, also on the temporal axis numerical results fit. As Okada's method reconstructs the initial earthquake from a known tsunami we expect accuracy on these levels.

Both events are simulated with adaptive mesh refinement along wave fronts, where our only criterion to detect those is the change relative in water height compared to the size of cell. Calm areas are coarsened again. An exemplary plot of the Sumatra tsunami with the refined grid can be seen in Fig. 13. Fig. 12 shows the actual tsunami after 60 min. Only recorded data available is tracked
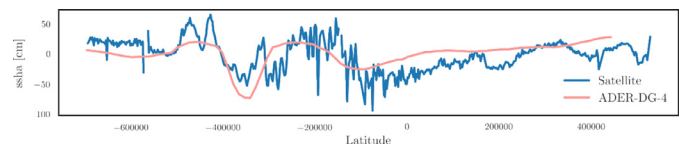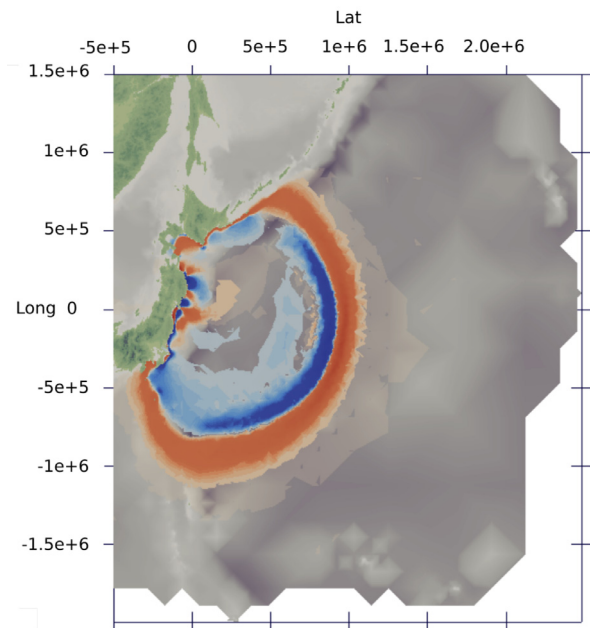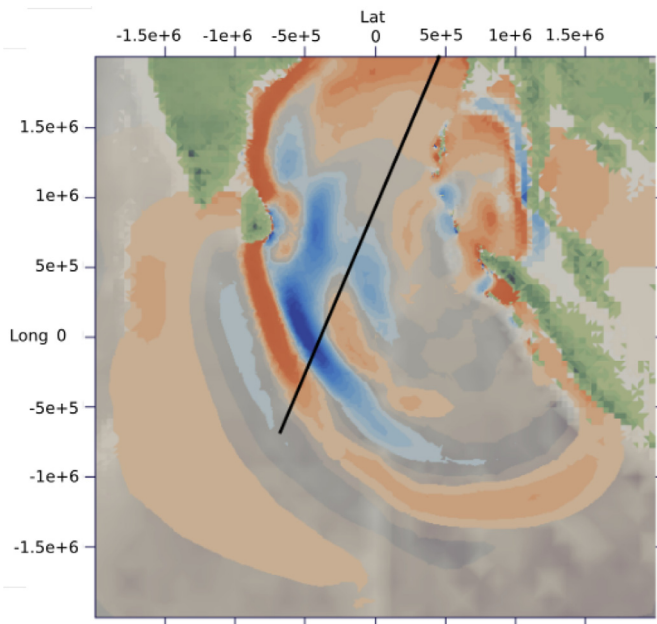
by the satellite Jason-1 at approximately 2 h after the event. The data set is a snapshot of a path through the tsunami. The comparison can be seen in Fig. 9. As initial data is not reconstructed from the tsunami itself numerical results show high dissipation. On the other hand results resemble the shape of the actual tsunami, as both peaks as well as the depth are hit.

7. Conclusion

We presented the application of an ADER-DG method on the simulation of tsunami waves. Our implementation is based on
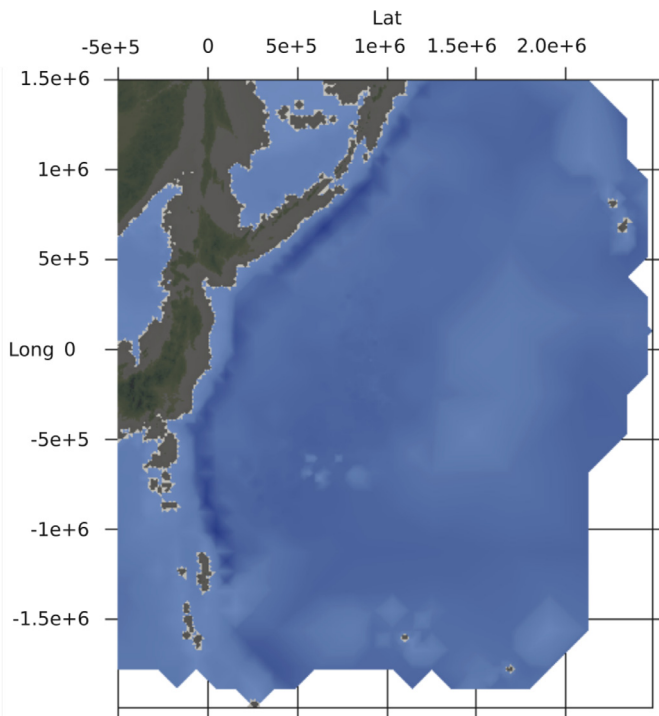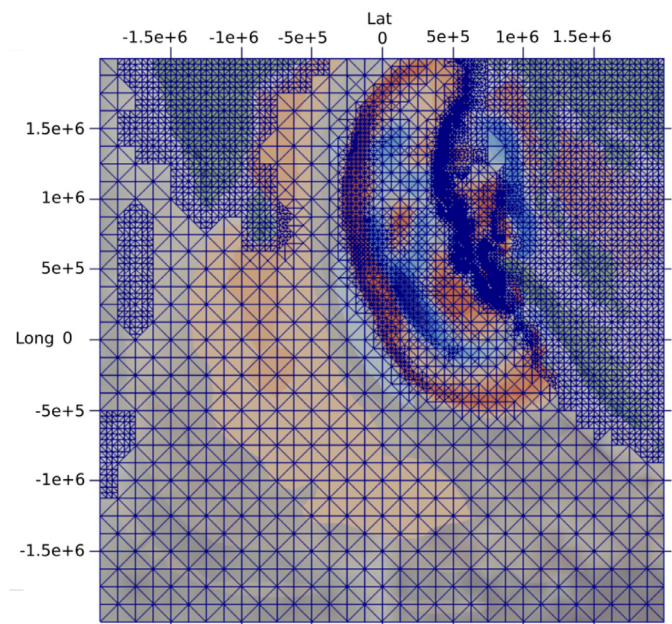
Fig. 11. Method plot for the Tohoku tsunami after 60 min. Blue areas indicate the ADER-DG method, grey FV patches. Shown in the background is the bathymetry of the area.

Fig. 13. Sumatra tsunami after 60 min. The current adaptive grid is shown in blue and shows high refinement in areas of perturbations. (For interpretation of the references to color in this figure legend, the reader is referred to the web version of this article.)

Considering the numerical results of Section 5, our method offers an option to simulate tsunamis with high-order convergence on open-ocean areas, while still being able to resolve coastlines. With the framework sam(oa)^2 our method has a powerful fundament for future large production runs on HPC systems. From the use of higher order, we also expect to leave the memory-bound regime of performance (compare [23]). As the computational intensive parts of our method are based on small dense matrix–matrix multiplications we see a high potential of optimization of node-level performance. Such an optimization will be necessary to show a comprehensive comparison of time-to-solution with other established methods.

Fig. 12. Sumatra tsunami after 120 min. The black line indicates the traversed route of the satellite while taking the snapshot of Fig. 9.

the sam(oa)^2 framework. We described modifications of the ADER-DG method to guarantee the well-balanced property, and implementation of the *a-posteriori* FV limiter which allows our high order scheme to resolve wetting & drying shorelines. Numerical tests verified our assumptions on high-order convergence and the well-balanced property. A comparison to a simple FV method showed the advantage in accuracy for practical use cases: two actual tsunami reconstructions were presented.

References

[1] George DL. Augmented Riemann solvers for the shallow water equations over variable topography with steady states and inundation. J Comput Phys 2008;227(6):3089–113. doi:10.1016/j.jcp.2007.10.027.

[2] Delis Argiris I. Improved application of the Hlle Riemann solver for the shallow water equations with source terms. Int J Numer Method Biomed Eng 2003;19(1):59–83.

[3] Vater S, Beisiegel N, Behrens J. A limiter-based well-balanced discontinuous Galerkin method for shallow-water flows with wetting and drying: one-dimensional case. Adv Water Resour 2015;85:1–13.

[4] Bunya S, Kubatko EJ, Westerink JJ, Dawson C. A wetting and drying treatment for the Runge–Kutta discontinuous Galerkin solution to the shallow water equations. Comput Methods Appl Mech Eng 2009;198(17):1548–62.

[5] Dumbser M, Balsara DS, Toro EF, Munz C-D. A unified framework for the construction of one-step finite volume and discontinuous Galerkin schemes on unstructured meshes. J Comput Phys 2008;227(18):8209–53. doi:10.1016/j.jcp.2008.05.025.

[6] Dumbser M, Loubre R. A simple robust and accurate a posteriori sub-cell finite volume limiter for the discontinuous Galerkin method on unstructured meshes. J Comput Phys 2016;319(Supplement C):163–99. doi:10.1016/j.jcp.2016.05.002.

[7] Dumbser M, Castro M, Parés C, Toro EF. ADER schemes on unstructured meshes for nonconservative hyperbolic systems: applications to geophysical flows. Comput Fluids 2009;38(9):1731–48.

[8] Meister O. Sierpinski curves for parallel adaptive mesh refinement in finite element and finite volume methods, München: Institut für Informatik, Technische Universität München; 2016. Dissertation.

[9] Meister O, Rahnema K, Bader M. Parallel memory-efficient adaptive mesh refinement on structured triangular meshes with billions of grid cells. ACM Trans Math Softw 2016;43(3). 19:1–19:27. doi:10.1145/2947668.

[10] Mitchell WF. Adaptive refinement for arbitrary finite-element spaces with hierarchical bases. J Comput Appl Math 1991;36(1):65–78.

[11] Bader M. Space-filling curves - an introduction with applications in scientific computing. Texts in computational science and engineering, 9. Springer-Verlag; 2013.

[12] Giraldo F, Hesthaven J, Warburton T. Nodal high-order discontinuous Galerkin methods for the spherical shallow water equations. J Comput Phys 2002;181(2):499–525. doi:10.1006/jcph.2002.7139.

[13] Xing Y, Shu C-W. High order finite difference WENO schemes with the exact conservation property for the shallow water equations. J Comput Phys 2005;208(1):206–27. doi:10.1016/j.jcp.2005.02.006.

[14] Hesthaven J, Warburton T. Nodal discontinuous Galerkin methods: algorithms, analysis, and applications. Texts in applied mathematics. Springer New York; 2007. ISBN 9780387720678.

[15] LeVeque RJ, George DL. High-resolution finite volume methods for the shallow water equations with bathymetry and dry states. Adv Numer Models Simulat Tsunami Waves Runup 2008;10:43–73.

[16] LeVeque RJ, George DL, Berger MJ. Tsunami modelling with adaptively refined finite volume methods. Acta Numerica 2011;20:211–89.

[17] Ghosh KK, Debnath L. Some exact solutions of non-linear shallow water equations. Int J Non Linear Mech 1997;32(3):633–6. doi:10.1016/S0020-7462(96)00072-8.

[18] Castro CE, Toro EF, Käser M. ADER scheme on unstructured meshes for shallow water: simulation of tsunami waves. Geophys J Int 2012;189(3):1505–20. doi:10.1111/j.1365-246X.2012.05471.x.

[19] Audusse E, Bouchut F, Bristeau M-O, Klein R, Perthame B. A fast and stable well-balanced scheme with hydrostatic reconstruction for shallow water flows. SIAM J Scient Comput 2004;25(6):2050–65. doi:10.1137/S1064827503431090.

[20] Okada T, Sugano T, Ishikawa T, Ohgi T, Takai S, Hamabe C. Structural design methods of buildings for tsunami resistance (SMBTR). The Building Center of Japan, Japan; 2005.

[21] Galvez P, Ampuero J-P, Dalguer L, Somala S, Nissen-Meyer T. Dynamic earthquake rupture modelled with an unstructured 3-d spectral element method applied to the 2011m 9 Tohoku earthquake. Geophys J Int 2014;198(2):1222–40.

[22] Uphoff C, Rettenberger S, Bader M, Madden EH, Ulrich T, Wollherr S, et al. Extreme scale multi-physics simulations of the tsunamigenic 2004 Sumatra megathrust earthquake SC '17: Proceedings of the international conference for high performance computing, networking, storage and analysis, Denver, CO, USA; 2017. Accepted

[23] Breuer A, Heinecke A, Rannabauer L, Bader M. High-order ADER-DG minimizes energy-and time-to-solution of SeisSol. In: International conference on high performance computing. Springer; 2015. p. 340–57.